Atmos. Chem. Phys. Discuss., 13, 30407–30452, 2013
www.atmos-chem-phys-discuss.net/13/30407/2013/
doi:10.5194/acpd-13-30407-2013

Atmospheric Chemistry and Physics Discussions

Total ozone trends and variability during 1979–2012 from merged datasets of various satellites

W. Chehade, J. P. Burrows, and M. Weber

Institute of Environmental Physics (IUP), University of Bremen, Bremen, Germany

Received: 8 October 2013 – Accepted: 4 November 2013 – Published: 21 November 2013

Correspondence to: W. Chehade (chehade@iup.physik.uni-bremen.de)

Published by Copernicus Publications on behalf of the European Geosciences Union.

Abstract

The study presents a long term statistical trend analysis of total ozone datasets obtained from various satellites. A multi-variate linear regression was applied to annual mean zonal mean data using various natural and anthropogenic explanatory variables that represent dynamical and chemical processes which modify global ozone distributions in a changing climate. The study investigated the magnitude and zonal distribution of the different atmospheric chemical and dynamical factors to long-term total ozone changes. The regression model included the equivalent effective stratospheric chlorine (EESC), the 11 yr solar cycle, the Quasi-Biennial Oscillation (QBO), stratospheric aerosol loading describing the effects from major volcanic eruptions, the El Niño/Southern Oscillation (ENSO), the Arctic and Antarctic Oscillation (AO/AAO), and accumulated eddy heat flux (EHF), the latter representing changes due to the Brewer–Dobson circulation. The total ozone column dataset used here comprises the SBUV/TOMS/OMI merged data (1979–2012) MOD V8.0, the SBUV/SBUV-2 merged V8.6 and the merged GOME/SCIAMACHY/GOME-2 (GSG) WFDOAS merged data (1995–2012). The trend analysis was performed for twenty six 5° wide latitude bands from 65° S to 65° N, the analysis explained most of the ozone variability. The results show that QBO dominates the ozone variability in the tropics (±7 DU) while at higher latitudes, the dynamical indices, AO/AAO and eddy heat flux, have substantial influence on total ozone variations by up to ±10 DU. Volcanic aerosols are only prominent during the eruption periods and these together with the ENSO signal are more evident in the Northern Hemisphere. The signature of the solar cycle is evident over all latitudes and contributes about 10 DU from solar maximum to solar minimum. EESC is found to be a main contributor to the long-term ozone decline and the trend changes after the end of 1990s. A positive significant trend in total ozone columns is found after 1997 (between 1 and 8.2 DU decade^{-1}) which points at the slowing of ozone decline and the onset of ozone recovery. The EESC based trends are compared with the trends obtained from the statistical piecewise linear trend (PWLT or hockey stick) model with

ACPD
13, 30407–30452, 2013

a turnaround in 1997 to examine the differences between both approaches. Similar and significant pre-turnaround trends are observed. On the other hand, our results do indicate that the positive PWLT turnaround trends are larger than indicated by the EESC trends, however, they agree within 2-sigma, thus demonstrating the success of the Montreal Protocol phasing out of the ozone depleting substances (ODS).

A sensitivity study is carried out by comparing the regression results, using SBUV MOD 8.0 merged time series (1979–2012) and a merged dataset combining TOMS/SBUV (1979–June 1995) and GOME/SCIAMACHY/GOME-2 ("GSG") WF-DOAS (Weighting Function DOAS) (July 1995–2012) as well as SBUV/SBUV-2 MOD 8.6 (1979–2012) in the regression analysis in order to investigate the uncertainty in the long-term trends due to different ozone datasets and data versions. Replacing the late SBUV merged data record with GSG data (unscaled and adjusted) leads to very similar results demonstrating the high consistency between satellite datasets. However, the comparison of the new SBUV merged Mod V8.6 with the V8.0 data showed somewhat smaller sensitivities with regard to several proxies, however, the EESC and PWLT trends are very similar. On the other hand, the new MOD 8.6 data in the PWLT model revealed a reduced ODS related upward trend after 1997.

1 Introduction

Total ozone changes reflect changes in lower stratospheric ozone that is governed by chemical and dynamical short-term as well as long-term variability. Global ozone amounts decreased severely between the eighties and the mid-nineties where it reached minimum values. This decline was mainly due to the impact of the uncontrolled anthropogenic emissions containing the halogens, chlorine and bromine (chlorofluorocarbons CFCs, halons), which depleted the stratospheric ozone through catalytic chemistry. The chemical processes involving the ozone depleting substances (ODS), in particular the heterogeneous reactions in the polar region (ozone hole), are well known and documented in previous studies (e.g. Solomon, 1999; Staehe-

ACPD
13, 30407–30452, 2013

lin et al., 2001) and ozone assessments (World Meteorological Organization, WMO, 1999, 2003, 2007, 2011; SPARC, 1998; Stratospheric Processes And their Role in Climate, SPARC, 1998). The ODS emissions were controlled by the implementation of the Montreal Protocol (1987) and its Amendments and Adjustments and global ozone levels showed a slowing in the decline and started to increase since mid-nineties in response to the phase out of ODS in the stratosphere (WMO, 2003, 2007, 2011 and references therein). Some studies on the other hand demonstrated a significant evidence of a decadal time scale influence of atmospheric dynamics on ozone variability during the decline till the mid-nineties (e.g. Hood and Soukharev, 2005; Wohltmann et al., 2007; Mäder et al., 2007; Harris et al., 2008) as well as the increase over northern latitudes afterwards (e.g. Reinsel et al., 2005; Dhomse et al., 2006; Wohltmann et al., 2007; Harris et al., 2008). Long-term variability of stratospheric ozone is also seen to be influenced by variations in solar radiation (Chandra and McPeters, 1994; Bojkov and Fioletov, 1995; Miller et al., 1996; Zerefos et al., 1997; McCormack et al., 1997; Hood, 1997; Ziemke et al., 1997; Lee and Smith, 2003; Soukharev and Hood, 2006; Fioletov, 2009) and aerosols injected in the stratosphere after volcanic eruptions (Hofmann and Solomon, 1989; Peter, 1997; Solomon, 1999).

Analysis of long-term changes in ozone in order to detect a statistically significant trend after the levelling off the ODS in the stratosphere requires the full understanding and proper accounting of all the processes contributing to decadal ozone variability, which induces considerable uncertainty in trend determination, and to quantify and separate the relative influence of chemical and dynamical contributors. Global and long-term total ozone measurements acquired from various satellite borne atmospheric chemistry sensors (multi-decadal dataset) are very useful to monitor and study the interannual and decadal ozone variability and to determine long term global trends.

Previous trend assessments modelled the response of ODS related signal in terms of linear trends based on the expected linear increase and phasing out of ODS. This statistical approximation of the ODS is well known as the piecewise linear trend (PWLT or hockey stick) model with a turnaround in the late 1990s, when the stratospheric

ACPD
13, 30407–30452, 2013

halogens (released from ODS) reached maximum. In this study we used multiple linear regression which is a standard trend analysis tool to quantitatively asses the observed total ozone variations due to different natural and anthropogenic influences (WMO, 2003, 2007, 2011 and references therein), with the long-term trend in ozone related to ODS described by the equivalent effective stratospheric chlorine function (EESC).

The aim of this paper is first to assess and update the global trends of ozone recovery and its statistical significance as expected from the turnaround and slow decrease in stratospheric halogen after measures introduced by the Montreal Protocol and amendments to phase out ODS. The trends are determined from a statistical analysis of thirty four year of total ozone data. The estimated EESC-based trends are compared with the trends obtained from PWLT analysis to assess the differences between the models as the latter is sensitive to adding more data after the turnaround point. Moreover, the same statistical analysis is applied to different consolidated ozone dataset to investigate the uncertainty in the long-term trends due to the use of different ozone satellite datasets.

In Sect. 2, the major chemical and dynamical processes contributing to ozone variability are briefly summarized. The zonal mean total ozone datasets of the merged TOMS/SBUV/OMI V8.0 (1979–2012), the SBUV/SBUV-2 merged V8.6 (1979–2012) and GOME/SCIAMACHY/GOME-2 (1995–2012) are briefly described in Sect. 3, and the multiple linear regression model applied to the zonal total ozone data is presented in the following section. Section 5 discusses the results in details and the estimates of the trends are introduced in Sect. 6. The sensitivity of using different ozone dataset in the regression are presented in Sect. 7, the last section presents the major conclusions drawn.

2 Main contributors to ozone variability

The various natural and anthropogenic processes representing the state of the atmosphere (dynamical and chemical), modify the global ozone distributions and conse-

ACPD
13, 30407–30452, 2013

quently contributing to its variability in a changing climate employed in the multiple linear regression, are displayed in Fig. 1.

The different processes are briefly summarized below.

2.1 Brewer–Dobson circulation

The ozone abundances in different regions of the atmosphere are determined by a balance between photochemical processes (production and loss), catalytic destruction and, transport. Ozone is produced in the tropical stratosphere but most of ozone is found at higher latitudes away from its production source. Ozone is transported through a slow atmospheric circulation in the lower to middle stratosphere that moves the upwelling air parcels from the tropics poleward, and then subsides in extratropics and high latitudes where it builds up. The circulation is a broad hemispheric-scale meridional overturning which is limited to the winter season and historically known as the Brewer–Dobson circulation (BDC). The main features of the poleward drift of air masses in stratosphere were inferred from Brewer (1949) and Dobson (1956) water vapor and ozone measurements, respectively.

This meridional circulation is driven by the planetary scale atmospheric waves (Rossby and gravity waves) which are generated in the troposphere and propagated upwards to the stratosphere (Haynes et al., 1991; Rosenlof and Holton, 1993; Newman et al., 2001; Plumb, 2002).

The influence of the meridional circulation in a given winter impacts the ozone variability well into spring and summer (Fioletov and Shepherd, 2003; Weber et al., 2011). In the polar region, the accumulation of the lower stratospheric ozone is strongly governed by the intensity of diabatic circulation; the stronger the intensity in the wintertime, the stronger is the meridional mixing and the diabatic descent. This increases the stratospheric temperatures which weakens the polar vortex and less ozone is destructed by heterogeneous reactions (Chipperfield and Jones, 1999; Fusco and Salby, 1999; Randel et al., 2002).

ACPD
13, 30407–30452, 2013

The winter accumulated lower stratosphere eddy heat flux is considered a good measure (proxy) of the inter-annual variability of ozone due to the BDC variations (Fusco and Salby, 1999; Newman et al., 2001; Randel et al., 2002; Dhomse et al., 2006; Weber et al., 2011).

The contribution of the large scale stratospheric circulation to ozone fluctuations can also be determined by other dynamical explanatory variables such as the dominant recurrent non-seasonal (with no particular periodicity) sea level pressure variation pattern north/south of 20° S/N latitude known as the Arctic Oscillation (AO) (or North Annular Mode, NAM) and Antarctic Oscillation (AAO) (or Southern Annular Mode, SAM) indices (Fusco and Salby, 1999; Hartmann et al., 2000; Appenzeller et al., 2000; Randel et al., 2002; Kiesewetter et al., 2010; Steinbrecht et al., 2001). The QBO phase (see later section) also influneces the wave propagation and relates to variability in the BDC (Baldwin et al., 2001).

2.2 Quasi-biennial oscillation

The equatorial stratosphere is characterized by a slow recurring variability in its zonal winds which influences the interannual variability of total ozone columns (Baldwin et al., 2001). The winds propagate downwards and alternatively changing (oscillating) in the strength and direction, i.e. reverse from easterly to westerly in the lower and middle stratosphere (~ 16–50 km) with an average period of about 28 months (Reed et al., 1961). The fluctuating winds are termed the quasi-biennial oscillation (QBO) (Angell and Korshover, 1964) and are the result from the upward propagating equatorial waves and mean-flow interaction in the stratosphere (Lindzen and Holton, 1968; Plumb, 1977).

A secondary meridional circulation by the QBO is induced and superimposed on the normal Brewer–Dobson circulation which either enhances or weakens the BDC depending on the phase of QBO. During the westerly phase, maximum diabatic cooling to space occurs and the air parcels sink leading to an increase in total ozone. This downward descent is balanced by air parcels rising in the extratropics (decrease in

ACPD
13, 30407–30452, 2013

total ozone) and an equator-ward drift that slows the BDC. During the easterly phase of the QBO, the induced circulation reverses. The QBO signal also affects the ozone variability at high latitudes (Bowman, 1989; Lait et al., 1989; Chandra and Stolarski, 1991) and even effects the distortion of wintertime stratospheric polar vortex by modulating the propagating extratropical wave flux or Eliassen–Palm flux (Dunkerton and Baldwin, 1991). This modulation is called the Holton–Tan effect (Holton and Tan, 1980) with largest signal in winter and spring (Tung and Yang, 1994; Randel and Cobb, 1994; Baldwin et al., 2001).

2.3 El Niño-Southern Oscillation

El Niño Southern Oscillation (ENSO) is a coupled atmospheric and tropical Pacific Ocean interaction phenomenon (zonal) of warming or cooling fluctuations in sea surface temperatures (SST) and alternating air surface pressure (SP) between the central/eastern and western tropical Pacific. El Niño events, the warmer phase, occur when the sea surface temperatures in the eastern tropical Pacific (South American coast) are warmer than average due to drift of warm waters from the western Pacific (Indonesia) resulting from the weakened easterly trade winds and occur about every 3 to 7 yr. The atmospheric component of the phenomenon (coincided with El Niño and termed "Southern Oscillation") represents the occurrence of lower sea-level pressure near Tahiti and higher sea-level pressure in Australia. During the La Niña the opposite occurs.

ENSO is the dominant source of interannual variability of tropical climate. Beside SST and SP oscillations, it induces interannual global scale changes in ocean currents, surface pressure, convections, atmospheric temperature and winds, clouds and precipitation, and impacts the chemistry of trace gases in the troposphere.

During the 1997/98 El Niño event, highest amounts of tropospheric column ozone (up to 25 DU increase) were registered in the tropics (Chandra et al., 1998; Fujiwara et al., 1999; Thompson et al., 2001), half of the increase were attributed to biomass burning over Indonesia during September–November 1997 and the remaining amounts

ACPD
13, 30407–30452, 2013

resulted from El Niño driven large scale changes in the ocean–atmosphere dynamics that transported ozone rich air from the stratosphere to the troposphere as reported by some modelling studies e.g. Sudo and Takahashi (2001); Chandra et al. (2002); Zeng and Pyle (2005). Ziemke et al. (2010) even proposed a new El Niño index derived from column ozone.

ENSO phases have a global impact, affecting the circulation in the extratropics by modulating the generation and propagation of Rossby wave which is strongly evident in the northern winter months (Trenberth et al., 2002). The warm phase is associated with stratospheric warming (van Loon and Labitzke, 1987; Labitzke and van Loon, 1999), and a strengthened BDC in the middle atmosphere yielding an enhanced upwelling of ozone-rich air from the tropics and a weaker polar vortex (Newman et al., 2001; Randel et al., 2002; Bronnimann et al., 2004; Manzini et al., 2006; Taguchi and Hartmann, 2006; Camp and Tung, 2007). ENSO results in temperature and ozone anomalies in the stratosphere that are opposite to the tropospheric anomalies.

2.4 Chlorine and bromine containing ODS

Anthropogenic halogenated substances (chlorofluorocarbons CFCs, halons) have been the principal source of stratospheric ozone depletion through catalytic chemistry over the past few decades (Stolarski and Cicerone, 1974; Molina and Rowland, 1974). Their very long atmospheric residence times allow them to be transported to the upper stratosphere where they photo-dissociate producing Cl and Br atoms which destroy ozone. Solomon (1999) presents a review of the key processes involved in ozone depletion.

The evolution of the long-lived ODS is a key parameter to describe long term ozone changes. Equivalent Effective Stratospheric Chlorine (EESC) index is used as a measure of the inorganic chlorine and bromine amounts accumulated in the stratosphere weighted by their ozone-destructive potential and fractional release rate (WMO, 1999, 2003, 2007, 2011). This is proportional to changes in total column ozone (Daniel et al., 1995). Stratospheric EESC is calculated from the surface measurements of

ACPD
13, 30407–30452, 2013

tropospheric ODS abundances taking into account the greater per-atom potency of stratospheric Br compared to Cl in its ozone destruction with a constant factor, α (EESC = Cl + $\alpha \cdot$ Br), conversion of Cl_y and Br_y, and for the transit times (or ages) the air takes to be transported from surface to different regions in the stratosphere. The implementation of Montreal Protocol and its Amendments and Adjustments, enacted in 1987, succeeded in reducing the abundances of the dominant ODS. EESC has levelled off through the late mid-nineties and afterwards started a slow decline. The EESC index has already been used in several ozone trends statistical models e.g., Newman et al. (2004); Fioletov and Shepherd (2005); Dhomse et al. (2006); Stolarski and Frith (2006); Randel (2007); Harris et al. (2008); Kiesewetter et al. (2010).

2.5 Solar cycle

Sun is the primary source of energy for Earth, any variation in the emitted energy output has a significant impact on climate and atmosphere (Lean and Rind, 2001; Rind, 2002; Haigh, 2003). Global total ozone amounts vary by 2 to 3 % during a solar cycle (WMO, 2003, 2007). Solar variability is considered as a dominant form of long-term ozone changes and has been included in all ozone trend assessments (WMO, 1999, 2003, 2007, 2011).

The variations of the solar ultraviolet spectral irradiance largely modify ozone photochemistry in the upper stratosphere (Brasseur, 1993). In the lowermost stratosphere, the solar cycle couples with QBO and modulates stratospheric circulation which indirectly effects ozone transport (Labitzke and van Loon, 1993; Kodera and Kuroda, 2002; Hood and Soukharev, 2003). In relation to the 11 yr solar cycle, a clear decadal response is detected in long-term ozone records and is in phase with it (Chandra and McPeters, 1994; Bojkov and Fioletov, 1995; Miller et al., 1996; Zerefos et al., 1997; McCormack et al., 1997; Hood, 1997; Ziemke et al., 1997; Lee and Smith, 2003; Soukharev and Hood, 2006; Fioletov, 2009).

ACPD
13, 30407–30452, 2013

2.6 Aerosols

Major volcanic eruptions inject large amounts of sulfate aerosols into the stratosphere that perturb stratospheric temperature and circulation and enhance catalytic ozone depletion through heterogeneous chemistry (Hofmann and Solomon, 1989; Peter, 1997; Solomon, 1999) releasing chlorine and bromine from ODS. The eruptions of the tropical volcanoes of El Chichón (Mexico, 1982) and Mt. Pinatubo (Philippines, 1991) were the major volcanic activities since the late 1970s. The volcanic aerosols were mixed relatively rapidly throughout the stratosphere in both hemispheres and sedimented out within couple of years. Stratospheric ozone reduced significantly following the eruptions in the Northern Hemisphere (Randel et al., 1995; Solomon et al., 1996; SPARC, 1998; WMO, 1999, 2003, 2007, 2011) which persisted for two to three years, while Southern Hemisphere ozone records did not show any pronounced ozone deficit (Fioletov et al., 2002; WMO, 2003, 2007, 2011). Several studies (Schnadt Poberaj et al., 2011; Aquila et al., 2013) showed that enhanced ozone transport through changes in dynamical processes counteracted the chemical losses.

3 Satellite total ozone time series

Zonal mean total ozone columns from the TOMS/SBUV/OMI Merged Ozone Dataset (MOD) Version 8.0 (Stolarski and Frith, 2006) were used in this study. This dataset combines data from eight independent backscatter ultraviolet technique (BUV-type) satellite instruments (Total Ozone Mapping Spectrometer TOMS, Solar Backscatter Ultraviolet SBUV/SBUV-2, and Ozone Monitoring Instrument OMI) with measurements from 1979 till 2012. Drifts and biases in overlapping periods among instruments were removed (Stolarski and Frith, 2006). For the sensitivity study, the SBUV/SBUV-2 Version 8.6 (MOD 8.6) ozone data product (1979–2012) were also used, the construction of the MOD V8.6 is based on the calibration and analysis processes presented in DeLand et al. (2012), Bhartia et al. (2012) and McPeters et al. (2013). Both MOD V8.0

ACPD
13, 30407–30452, 2013

and V8.6 can be obtained from http://acd-ext.gsfc.nasa.gov/Data_services/merged/. In this study we also used the merged GOME/SCIAMACHY/GOME-2 (GSG) total ozone dataset. This dataset extends from 1995 to 2012 and combines data from GOME (1995–2003) (Coldewey-Egbers et al., 2005; Weber et al., 2005), SCIAMACHY (2002–2006) (Bracher et al., 2005) and GOME-2 (2007–present) (Weber et al., 2007). GOME was very stable over the operational period (1995–2012) and selected as a reference for bias adjusting SCIAMACHY and GOME-2 data (Kiesewetter et al., 2010; Weber et al., 2011, 2012). Adjustments were made by determining a mean scaling factor (GOME-2 and SCIAMACHY) from the monthly mean zonal mean ozone ratio with respect to GOME. The data can be obtained from http://www.iup.uni-bremen.de/gome/wfdoas/merged/. Figure 2 shows annual means of the area-weighted total ozone columns over the period 1979–2012 of the different global datasets used in this study and the ground-based measurements which combines Brewer, Dobson, and filter spectrometer data for various zonal bands: global (60° S – 60° N), middle latitudes in both hemispheres (35–60°) and the tropics (25° S – 25° N), respectively.

4 Multivariate linear regression

Trends in global total ozone are investigated through a multivariate linear regression model consisting of various explanatory parameters (as discussed above) which account for chemical and dynamical processes in the atmosphere. This statistical method has been frequently used in ozone assessments (Bojkov et al., 1990; SPARC, 1998, 2010; WMO, 1999, 2003, 2007, 2011, and references therein) in order to assess the contributions of various natural and anthropogenic changes to long-term and short-term variability of ozone. The annual mean total ozone column (TOZ) time series is

ACPD
13, 30407–30452, 2013

constructed as a simple linear sum of explanatory variables time series as follows:

$$\begin{aligned}\mathrm{TOZ}(n) = \mathrm{TOZ}(n)^{\circ} &+ \alpha^{\mathrm{EESC}} \cdot \mathrm{EESC}(n) \\ &+ \alpha^{\mathrm{qbo}} \cdot \mathrm{qbo}(n) \\ &+ \alpha^{\mathrm{solar}} \cdot \mathrm{solar}(n) \\ &+ \alpha^{\mathrm{aer}} \cdot \mathrm{aer}(n) \\ &+ \alpha^{\mathrm{ENSO}} \cdot \mathrm{ENSO}(n) \\ &+ \alpha^{\mathrm{AO/AAO}} \cdot \mathrm{AO/AAO}(n) \\ &+ \alpha^{\mathrm{EHF}} \cdot \mathrm{EHF}(n) \\ &+ \varepsilon(n) \end{aligned} \quad (1)$$

where n is a running index (from zero to 34) corresponding to all years during the period 1979–2012 while α^X represent the time dependent regression coefficients of each proxy (X) and ε is the residual or noise time series. The EESC concentration were obtained from NASA Goddard Space Flight Center web site (http://acdb-ext.gsfc.nasa.gov/Data_services/automailer/index.html) and were calculated for a mean age of air of three years and width of age-of-air distribution of one and half years (Newman et al., 2006, 2007) and bromine efficiency of $\alpha = 60$ was used (Sinnhuber et al., 2009). Equatorial zonal winds at 10 and 30 hPa pressure levels (from FU Berlin, http://www.geo.fu-berlin.de/en/met/ag/strat/produkte/qbo/index.html) were used to provide the QBO index in the regression analysis. QBO at 10 and 30 hPa are out of phase ($\sim \pi/2$, Bojkov and Fioletov, 1995; Steinbrecht et al., 2003) and account for the effect of QBO strength and phase on ozone at different latitudes. This obviates the need to find the optimal time lag since the effect on ozone in the extratropics is represented by an optimal lag relation (Bojkov et al., 1990).

To account for the effect of volcanic aerosols after El Chichón and Mount Pinatubo eruptions, time dependent stratospheric aerosol optical depth at 550 nm (Sato et al., 1993) is used. The optical depth (http://data.giss.nasa.gov/modelforce/strataer/) is

ACPD
13, 30407–30452, 2013

multiplied by the stratospheric chlorine content (EESC) (Wohltmann et al., 2007). To investigate the impact of UV solar irradiance modulation related to the 11 yr solar cycle, core-to-wing ratio of the MgII line at 280 nm (http://www.iup.uni-bremen.de/gome/) as well as solar radio flux at 10.7 cm wavelength (ftp://ftp.ngdc.noaa.gov/STP/space-weather/solar-data/solar-features/solar-radio/noontime-flux/pentiction/pentiction_adjusted/listings/listing_drao_noontime-flux-adjusted_daily) are used as proxies. For the El Niño Southern Oscillation phenomenon, the Nino 3.4 index (http://www.cpc.ncep.noaa.gov/data/indices/ersst3b.nino.mth.81-10.ascii) is included in the regression. The AO/AAO index is obtained from NOAA National Weather Service Climate Prediction Center web site (http://www.cpc.ncep.noaa.gov/products/precip/CWlink/daily_ao_index/teleconnections.shtml) and the extratropical 100 hPa eddy heat flux (EHF) averaged over midlatitudes between 45° and 75° in each hemisphere is obtained from ECMWF ERA-Interim as described by Weber et al. (2011).

The explanatory variables time series used in a multivariate linear trend analysis must be fully independent (uncorrelated); in this study the correlations between predictors are small (between 0.1 and 0.2) except for the aerosol and ENSO term (0.34). In order to account for auto-regression, a Cochrane–Orcutt transformation (Cochrane and Orcutt, 1949) is applied to the regression. The transformation does not change the estimates of the fitting coefficients, however, the fitting errors increase due to the reduction in degree of freedom.

5 Results

The regression analysis (Eq. 1) is applied to TOMS/SBUV/OMI annual mean zonal mean total ozone data from 65° S to 65° N in steps of 5°. An example of the model and the contributions (in Dobson Units, DU) of the different natural as well as anthropogenic explanatory variables are illustrated in Fig. 3 for the 60–65° N latitude band. The regressed ozone time series (blue, first panel) fits well to the ozone measurements (red) and follows the general features capturing the decline of ozone to the mid-1990s,

ACPD
13, 30407–30452, 2013

the pronounced ozone losses after the Mt. Pinatubo eruption and the slow increase after that. The black curve (EESC) describes long-term variations attributed to anthropogenic emissions of ODS. After 1997, a small increase (3.3 ± 0.8 DU decade^{-1}) is attributed to the EESC decline. The regression fit shows a correlation (r) of 0.78 between modelled and measured total ozone, while the coefficient of determination, i.e R^2 (the ratio of the variance of all terms in Eq. (1) to the total variance), is 0.63. This implies that about 63 % of the observed variance of total ozone column can be explained by the regression.

The green line in the second panel displays the regression residuals between measured and regressed data (in percent). The fitted signal of each explanatory parameter $\alpha^X \cdot X$ is shown in the third to seventh panel of Fig. 3. The overall combined QBO related component (black, $\alpha^{\text{qbo10}} \cdot \text{qbo10} + \alpha^{\text{qbo30}} \cdot \text{qbo30}$) comprises the highest contribution to interannual ozone variability, the fluctuation from easterly to westerly QBO phase at 10 hPa (red) and 30 hPa (blue) attributes around 14 DU. The 11 yr solar cycle contribution (blue, MgII index) reaches about 13 DU from solar minimum to solar maximum. The aerosol response associated with El Chichón and Mount Pinatubo eruptions (orange) accounts for about 11 DU and 15 DU loss in total ozone in 1983 and 1992, respectively. The influence of ENSO (turquoise) is typically about ±8 DU, whereas the 1997/98 El Niño event contributed up to +4 DU. Eddy heat flux related ozone contribution (magenta) amounts ±4 DU while the negative and positive phases of AO/AAO oscillation (lime-green) contribute ±5 DU. Both dynamical proxies were included in the analysis as the regression model worked better and improved the correlation and the coefficient of determination (not shown here). The regression coefficients of the various proxies along with the standard deviation (in brackets) are noted as well in the plot.

The residual circulation transports more stratospheric ozone in winter and the wintertime ozone anomalies remain evident till autumn. Weber et al. (2011) reported positive correlation between spring-to-fall ozone ratio and the winter mean eddy heat flux above and below 50° S/N, while in the tropics (till 40° S/N) the relation is anti-correlated. To account for ozone wintertime build up and its persistence through the summer, winter

ACPD
13, 30407–30452, 2013

mean of eddy heat flux (from October of the previous year until March (NH) and April to September (SH)) are used in the regression equation (Eq. 1) instead of the annual mean used in Fig. 3. Figure 4 displays the regression results for the same latitude band as in Fig. 3 but using the winter mean eddy heat flux. The ozone reconstructions and contributions of EESC, QBO, solar cycle, aerosols and ENSO show the same features and patterns as in Fig. 3, respectively. The R^2 has now improved to 0.76, correlation is about 0.87 and the residual mean square (rms, the sample estimate of the variance of the regression residuals) is 5.6 DU.

Moreover, the choice of wintertime dynamical EHF has a significant impact on the effect of the solar cycle, aerosols, ENSO and EHF processes since the contributions of aerosols, ENSO and EHF are statistically significant at 2σ level and explain most of the observed ozone variations. The corresponding amplitudes of total ozone variation increased by almost 70 % for aerosol and ENSO terms, and by 75 % for solar cycle and EHF terms, with highest contribution to total ozone variability arising from EHF reaching about 20 DU. The AO terms are now not statistically significant (as they are most likely represented in the eddy heat flux term). The linear trend after 1997 due to the ODS declines remained unchanged.

The statistical trend model was applied to twenty six 5° wide latitude mean ozone data bands from 65° S to 65° N. The measured and modelled ozone are displayed in Fig. 5 for each latitude band. The reconstructed ozone generally captures the temporal ozone variations and follows the general features of the slow decline till the mid-nineties and the increase after that. The residuals (violet, right scale of the panels) are typically within 3 %. The correlation, R^2 and rms are also displayed for each latitude band.

The effect of each proxy on the interannual variability of total ozone measurements is also estimated. Figure 6 shows the estimates of fitting coefficients of the different explanatory variables (using the same color notation as in Figs. 3 and 4) for each latitude band as obtained from the regression analysis. The top panel displays the correlation between measured annual ozone and regression results. Typical values are higher than 0.8 across all latitude bands. The model works well with the choice of

ACPD
13, 30407–30452, 2013

the terms included in the regression since the values of R^2 are larger than 0.6. This indicates that the statistical model explains the major part of the total ozone variance, in the tropics (within 5° S/N). In southern subtropics the regression describes the total ozone variations almost completely.

The second panel shows the total ozone response related to ODS abundance in the selected latitude bands as represented by the EESC term. The EESC coefficient increases in magnitude with increasing latitude. In the inner tropics the EESC trends are zero. The EESC response is larger in the Southern Hemisphere as compared to the same latitudes in the Northern Hemisphere latitudes. The largest ozone loss attributed to the chemical ozone depletion by the accumulated anthropogenic ODS, are found south of 50° S in the "ozone hole" region. This indicates that the Antarctic ozone loss has a higher impact on the long-term decline at Southern Hemisphere midlatitudes (Chipperfield, 2003; Fioletov and Shepherd, 2005; Kiesewetter et al., 2010). The error bars indicate the statistical significance at two sigma level (95 % significance level). The EESC term is statistically significant in all latitude bands except the tropics (north of 20° S and south 20° N).

The total QBO coefficient is symmetric about the equator (shown in black in the third panel) and dominates ozone variability in the tropical and southern sub-tropical regions with highest and clear influence between 5° S and 5° N latitude bands while it is insignificant in the northern subtropics. Not unexpected, the 30 hPa QBO term is dominating over the 10 hPa QBO term. The QBO phase change from the equator to the subtropics are due to a secondary circulation with the downward branch in the tropic and the upwelling branch in the subtropics (positive ozone anomalies in the tropics and negative in the 20–50° S/N subtropical regions).

The solar coefficients are statistically significant. When the core-to-wing ratio of the MgII line is replaced by the solar radio flux at 10.7 cm as a solar proxy in the regression model (Eq. 1), the same ozone signal between solar maximum and solar minimum was found and did not alter the influence of other processes (not shown here) as well as the correlation, determination coefficient and rms.

ACPD
13, 30407–30452, 2013

The coefficients of stratospheric aerosols (orange) in the fifth panel, are mostly negative and increases with increasing latitude. El Chichón and Mt. Pinatubo eruptions significantly influence total ozone over the northern latitudes and the negative ozone signal is in good agreement with results reported in previous studies (Staehelin et al., 1998; Fioletov et al., 2002; Mäder et al., 2007; Wohltmann et al., 2007; Harris et al., 2008; Rieder et al., 2010a, b, 2011; WMO, 2007, 2011). At southern mid-latitudes the signal is unexpectedly positive. Similar results were noted by (Fioletov et al., 2002) and were also documented in the WMO reports (WMO, 2003, 2007, 2011). This spatial pattern emanates from the dynamical processes in which enhanced ozone transport to southern mid-latitudes driven by strong warm ENSO phase and negative AAO accompanied by the shifting and stretching of the vortex towards the Antarctic Peninsula suppressed the ozone signal (Schnadt Poberaj et al., 2011; Aquila et al., 2013; Rieder et al., 2013).

The sixth panel shows the distribution of the ENSO coefficient over the studied latitude range. A significant moderate negative influence on total ozone is centered over the tropical region (15° S–5° N). The positive patterns in the northern high latitudes are interpreted as consequences of enhanced transport from the tropics during warm ENSO events (Frossard et al., 2013; Rieder et al., 2013) while the coefficient are statistically insignificant towards southern high latitudes.

The AO estimates are found to be significant over the northern latitudes with large positive coefficients in the sub-tropics decreasing the total ozone column ozone during the positive phase of AO and large negative coefficients enhancing ozone during the negative phases of AO in the extra-tropics. The extremely negative AO index in 2010 resulted in very high ozone throughout the northern extratropics (Steinbrecht et al., 2001). Similar to the NH, the negative AAO phases enhances SH ozone transport, however, the AAO contribution at high southern latitudes in the regression is statistically not significant except for the 50–60° S region.

The winter mean eddy heat coefficients are statistically significant and dominates ozone variability in the higher latitudes of both hemispheres above 50°.

ACPD
13, 30407–30452, 2013

6 ODS related trends in ozone total column

Ozone trends related to ODS are calculated for all latitude bands according to the full regression model (Eq. 1). Based on the EESC curves, two clear linear trends can be estimated. A decline in ozone amounts starting at the beginning of the measurements due to the increases in stratospheric ODS loading (0.447 ppbv decade^{-1}) till the turnaround of the ODS levels in 1997 (EESC maximum), and a negative trend following the levelling-off and phase out of ODS in the stratosphere (−0.179 ppbv decade^{-1}) accompanied with an increase in total column levels. Both phases of the ODS related ozone trends can be approximated as the slopes of the declining and increasing phases of EESC multiplied by the EESC coefficient (DU decade^{-1}).

The negative until 1997 and positive turnaround after 1997 (red solid circles) EESC-based trends as a function of latitude are displayed in the bottom panel of Fig. 7. The positive trends after 1997 increase in magnitude with latitude and are statistically significant across nearly all latitude bands except the tropics (south of 20° N and north 20° S). In the northern sub-tropics and extra-tropics, the positive trends are smaller than those in southern counterparts. This can be explained by the large dynamically driven variations dominating the ozone variability in northern latitudes (Reinsel et al., 2005; Dhomse et al., 2006; Wohltmann et al., 2007; Harris et al., 2008). The statistically significant trends can be attributed to the onset of anthropogenic (or ODS related) ozone recovery after 1997.

The ozone trends before and after the ODS turnaround can also be described by calculating piecewise linear trends (PWLT or hockey stick) (Reinsel et al., 2002, 2005; Newchurch et al., 2003; Miller et al., 2006; Vyushin et al., 2007, 2010; Yang et al., 2009). The PWLT model replaces the EESC term ($\alpha^{\mathrm{EESC}} \cdot \mathrm{EESC}(n)$) in Eq. (1) by two separate linear trend terms:

$$\alpha^{\mathrm{EESC}} \cdot \mathrm{EESC}(n) = \alpha^{t_1} \cdot \delta(\leq 1997) + \alpha^{t_2} \cdot \delta(> 1997) \quad (2)$$

As for the EESC regression, the results obtained from the PWLT model (not shown here) showed the same patterns as in Fig. 6 with the correlation and coefficient of

ACPD
13, 30407–30452, 2013

determination better than 0.82 and 0.73, respectively, the contributions of the other explanatory variables slightly altered. The MgII coefficient increased in the sub-tropics of both hemispheres (10–15 %), the eddy heat flux coefficient increased by 5–10 % in southern latitudes while in the northern latitudes it decreased largely and is statistically significant only north of 55° N. The AO coefficient is smaller (15–30 %) in 10–35° N bands and higher (35 %) in 40–50° N bands when PWLT is used.

Both of the above mentioned approaches equally well describe the total ozone changes during the last thirty years. Both EESC and PWLT related trends before and after 1979 are shown in Fig. 7.

Both EESC and PWLT trends before 1997 are close to each other and agree within the 2-sigma error bars (grey shades for PWLT and dashed lines for EESC). The positive trends after 1997 are almost identical south of 40° S and north of 50° N (statistically insignificant) while elsewhere, larger differences are observed. The post-1997 PWLT trend in the low to middle latitudes are up to four times larger than the EESC based trend but agree within the 95 % error bars (except 15–30° N). The PWLT trend after 1997 are larger than expected and cannot be accounted as a full true response to the ODS decline after 1997 since PWLT regression analysis is very sensitive to the length of the data record after 1997 (Vyushin et al., 2010). As the ODS related upward trend is fairly small, the PWLT is more strongly affected by uncertainties in the short-term variability.

7 Quality of satellite ozone data record

In this study, the merged WFDOAS GOME/SCIAMACHY/GOME-2 (GSG, 1995–2012) zonal total ozone dataset (Kiesewetter et al., 2010; Weber et al., 2011, 2012) and SBUV/SBUV-2 Version 8.6 (V8.6) ozone data product (1979–2012) (DeLand et al., 2012; McPeters et al., 2013) were also analysed in the regression model (Eq. 1, with wintertime eddy heat flux) to investigate the uncertainty in the long-term trends due to the use of different ozone datasets. The statistical analysis was applied for the same

ACPD
13, 30407–30452, 2013

latitude range (65° S–65° N). The GSG data (July 1995–December 2012) was combined with TOMS/SBUV data (January 1979–June 1995) without adjustments of the GSG data. The results as a function of latitude are depicted in blue in Figs. 8 and 9 together with the results for SBUV/SBUV-2 Version 8.6 dataset in green and the previous results for the TOMS/SBUV/OMI MOD 8.0 merged data (1979–2012) presented in red. The new results are generally in good agreement with the TOMS/SBUV/OMI results. For the GSG/MOD data in comparison to MOD V8, the correlation and determination coefficient are close in the tropics but decrease at higher latitudes. The GSG/MOD V8 rms are slightly lower within 10° N–40° N and slightly higher elsewhere. The differences when replacing part of the MOD V8 data with GSG data are very small indicating excellent agreement between both datasets. On the other hand, the correlation, coefficient of determination as well as rms for MMOD 8.6 improved between 25° S and 25° N latitiude range while south of 25° S the values slightly dropped and north of 25° N the values remained almost un changed.

The fit coefficients of the GSG/MOD V8 and MOD V8.6 data follow the same pattern as that for the MOD 8.0 merged dataset and agree within 2-sigma (see Fig. 9). The EESC trends and QBO estimates agree well and are within ±15 % with TOMS/SBUV/OMI estimates while ENSO generally changed by 15–30 %. The other signals are significantly altered by the use of the GSG and MOD 8.6 data. The MgII and aerosol signals obtained for GSG data are statistically insignificant north of 45° N and between 20° N and 40° N, respectively, and the eddy heat flux is only statistically significant north of 50° N and south of 60° S while AO estimates decreased up to 25–55 % in the subtropics.

Nevertheless, within 2-sigma fit parameters for all datasets agree. In particular, the EESC trends are almost identical. This means hat the GSG, MOD 8.0 and MOD 8.6 datasets are highly consistent.

The piecewise linear trend is applied to the SBUV/SBUV-2 MOD 8.6 data and the quality of the PWLT fit and the trends in comparison with the EESC trend regression model are shown in Fig. 10. The fit is almost identical in the 40° S–30° N latitude range,

ACPD
13, 30407–30452, 2013

slight changes are observed outside the latitude range. The pre-turnaround trends before 1979 for both EESC and PWLT approaches are very close to each other. On the other hand, the positive trends after 1997 are also close to each other, the values of the PWLT trend dropped significantly south of 40° S. Moreover, the positive PWLT is statistically insignificant over the latitude bands except for the narrow band 20–30° in each hemisphere. Figure 11 shows a comparison between the EESC and PWLT trend models for both MOD 8.0 and 8.6 datasets. The PWLT after 1997 is smaller for MOD V8.6 data than that for MOD V8, but agree within 2-sigma. Except for high southern latitudes, the PWLT and EESC trend after 1997 for MOD V8.6 data agree very well. The MOD V8 data showed generally larger post-1997 PWLTs than post-1997 EESC trends, but differences are only statistically significant in the northern subtropics.

8 Summary and conclusions

In this study, long-term evolution of zonal mean annual mean total ozone measurements from merged datasets of various satellites over the period 1979–2012 in 5° zonal bands between 65° S and 65° N were analysed by multiple linear regression. The regression analysis included different explanatory variables representing dynamical and chemical processes that modify global ozone distributions such as QBO, solar cycle, aerosols, ENSO, eddy heat flux, AO/AAO and the EESC terms. The TOMS/SBUV/OMI merged data were analysed first. The regression model explained about 60–95 % of the ozone variability across the considered latitude range. The QBO signal dominates the tropical region and contributes up to ±7 DU depending on its phase while at higher latitudes the eddy heat flux signal (±10 DU) and to lesser extent the ENSO and AO/AAO signals represent the major attribution to ozone variations. The effects of El Chichón (1982) and Mt. Pinatubo (1991) are limited to the periods of volcanic eruptions and are responsible for a large fraction of ozone loss (up to −14 DU and −22 DU, respectively), the signal is more prominent and statistically significant in the Northern Hemisphere.

ACPD
13, 30407–30452, 2013

The signature of the 11 yr solar cycle is evident over all latitude bands and the contribution to ozone variability can reach about 13 DU from solar maximum to solar minimum. Replacing the MgII index by the F10.7 cm proxy, does not change the ozone signal of the other explanatory variables or the statistical significance of the model although the Mg II index is believed to correlate better with solar UV irradiance changes than the F10.7 cm solar flux (Viereck et al., 2001, 2004).

Figure 5 shows that the EESC function is the dominant cause of long-term ozone decline in the stratosphere before 1997 and an increase afterwards. The trend is statistically significant and indicates the onset of ozone recovery as expected from the slow decrease in the stratospheric halogen after measures introduced by the Montreal Protocol and amendments to phase out the ODS. The comparison with the trends obtained from PWLT model yields similar results for the long-term decline before 1997. On the other hand, the positive PWLT turnaround trends are larger than the EESC trend at northern middle latitudes. The observed ozone changes are as expected from the turnaround in the ODS since 1997, however, the large year-to-year variability still masks the exact magnitude of the recent (and weak) ODS related trend.

A sensitivity study was carried out by comparing the results obtained from the regression model (Eq. 1) replacing the late MOD 8.0 data after 1995 with the merged GOME/SCIAMACHY/GOME-2 WFDOAS dataset (Kiesewetter et al., 2010; Weber et al., 2011, 2012) and SBUV/SBUV-2 MOD 8.6 ozone data from 1979 till 2012 (DeLand et al., 2012; McPeters et al., 2013). This allows us to assess the uncertainty which may arise form the observational data record. Although, some changes in the individual fit parameters were found, within the 2-sigma error bars the results were identical. This is in agreement with an earlier study by Kiesewetter et al. (2010) which also showed a high consistency between the GSG and the merged SBUV V8.0 data. In particular, the EESC related ozone trend is almost identical for the different total ozone datasets, so that the data quality of total ozone data appears to be not an issue here. The PWLT after 1997 is generally higher than the linear part of the EESC trend but except for the northern subtropics they agree within 2sigma. The MOD V8.6 data show

ACPD
13, 30407–30452, 2013

better agreement of the PWLT with the post-1997 EESC trend, however, the PWLT is for most regions not statistically significantly different from a zero trend. In summary, the updated trends up to end of 2012 consolidate the results from other studies (e.g. Mäder et al., 2010) that the observed trend change since 1997 proves the effectiveness of the Montreal Protocol phasing out ODS depleting substances. Since the ODS decline is now fairly slow (Fig. 1), the recent extratropical annual mean total ozone trends are strongly influenced by large year-to-year variability in atmospheric dynamics.

Acknowledgements. The authors acknowledge S. Frith, R. Stolarski and the NASA TOMS and SBUV instrument teams for the NASA MOD product used in this study. Part of this study was funded by the DFG Research Unit SHARP (SHARP-OCF).

References

Angell, J. K. and Korshover, J.: Quasi-biennial variations in temperature, total ozone, and tropopause height, J. Atmos. Sci., 21, 479–492, 1964. 30413

Appenzeller, C., Weiss, A. K., and Staehelin, J.: North Atlantic Oscillation modulates total ozone winter trends, Geophys. Res. Lett., 27, 1131–1134, 2000. 30413

Aquila, V., Oman, L. D., Stolarski, R., Douglass, A. R., and Newman, P. A.: The response of ozone and nitrogen dioxide to the eruption of Mt. Pinatubo at southern and northern midlatitudes, J. Atmos. Sci., 70, 894–900, 2013. 30417, 30424

Baldwin, M., Gray, L., Dunkerton, T., Hamilton, K., Haynes, P., Randel, W., Holton, J., Alexander, M., Hirota, I., Horinouchi, T., Jones, D., Kinnersley, J., Marquardt, C., Sato, K., and Takahashi, M.: The quasi-biennial oscillation, Rev. Geophys., 39, 179–229, 2001. 30413, 30414

Bhartia, P. K., McPeters, R. D., Flynn, L. E., Taylor, S., Kramarova, N. A., Frith, S., Fisher, B., and DeLand, M.: Solar Backscatter UV (SBUV) total ozone and profile algorithm, Atmos. Meas. Tech., 6, 2533–2548, doi:10.5194/amt-6-2533-2013, 2013. 30417

Bojkov, R. D. and Fioletov, V. E.: Estimating the global ozone characteristics during the last 30 years, J. Geophys. Res., 100, 16537–16552, 1995. 30410, 30416, 30419

Bojkov, R. D., Bishop, L., Hill, W. J., Reinsel, G. C., and Tiao, G. C.: A statistical trend analysis of revised Dobson Total Ozone data over the Northern Hemisphere, J. Geophys. Res., 95, 9785–9807, 1990. 30418, 30419

ACPD
13, 30407–30452, 2013

Bowman, K. P.: Global patterns of the quasi-biennial oscillation in total ozone, J. Atmos. Sci., 46, 3328–3343, 1989. 30414
Bracher, A., Lamsal, L. N., Weber, M., Bramstedt, K., Coldewey-Egbers, M., and Burrows, J. P.: Global satellite validation of SCIAMACHY O_3 columns with GOME WFDOAS, Atmos. Chem. Phys., 5, 2357–2368, doi:10.5194/acp-5-2357-2005, 2005. 30418
Brasseur, G.: The response of the middle atmosphere to long-term and short-term solar variability: a two-dimensional model, J. Geophys. Res., 98, 23079–23090, 1993. 30416
Brewer, A. W.: Evidence for a world circulation provided by the measurements of helium and water vapour distribution in the stratosphere, Q. J. Roy. Meteor. Soc., 75, 351–363, 1949. 30412
Bronnimann, S., Luterbacher, J., Staehelin, J., Svendby, T., Hansen, G., and Svenoe, T.: Extreme climate of the global troposphere and stratosphere in 1940–42 related to El Niño, Nature, 431, 971–974, doi:10.1038/nature02982, 2004. 30415
Camp, C. D. and Tung, K.-K.: Stratospheric polar warming by ENSO in winter: a statistical study, Geophys. Res. Lett., 34, L04809, doi:10.1029/2006GL028521, 2007. 30415
Chandra, S. and McPeters, R.: The solar cycle variation of ozone in the stratosphere inferred from NIMBUS 7 and NOAA 11 satellites, J. Geophys. Res., 99, 20665–20671, 1994. 30410, 30416
Chandra, S. and Stolarski, R. S.: Recent trends in stratospheric total ozone: implications of dynamical and El Chichón perturbations, Geophys. Res. Lett., 18, 2277–2280, 1991. 30414
Chandra, S., Ziemke, J. R., Min, W., and Read, W. G.: Effects of 1997–1998 El Niño on tropospheric ozone and water vapour, Geopshy. Res. Lett., 25, 3867–3870, 1998. 30414
Chandra, S., Ziemke, J. R., Bhartia, P. K., and Martin, R. V.: Tropical tropospheric ozone: implications for dynamics and biomass burning, J. Geophys. Res., 107, 4188, doi:10.1029/2001JD000447, 2002. 30415
Chipperfield, M. P.: A three-dimensional model study of long-term mid-high latitude lower stratosphere ozone changes, Atmos. Chem. Phys., 3, 1253–1265, doi:10.5194/acp-3-1253-2003, 2003. 30423
Chipperfield, M. P. and Jones, R. L.: Relative influences of atmospheric chemistry and transport on arctic ozone trends, Nature, 400, 551–554, 1999. 30412
Cochrane, D. and Orcutt, G. H.: Application of least squares regression to relationships containing autocorrelated error terms, J. Amer. Stat. Assoc., 44, 32–61, 1949. 30420

ACPD
13, 30407–30452, 2013

Coldewey-Egbers, M., Weber, M., Lamsal, L. N., de Beek, R., Buchwitz, M., and Burrows, J. P.: Total ozone retrieval from GOME UV spectral data using the weighting function DOAS approach, Atmos. Chem. Phys., 5, 1015–1025, doi:10.5194/acp-5-1015-2005, 2005. 30418
Daniel, J. S., Solomon, S., and Albritton, D.: On the evaluation of halocarbon radiative forcing and global warming potentials, J. Geophys. Res., 100, 1271–1285, 1995. 30415
DeLand, M. T., Taylor, S. L., Huang, L. K., and Fisher, B. L.: Calibration of the SBUV version 8.6 ozone data product, Atmos. Meas. Tech., 5, 2951–2967, doi:10.5194/amt-5-2951-2012, 2012. 30417, 30426, 30429, 30443
Dhomse, S., Weber, M., Wohltmann, I., Rex, M., and Burrows, J. P.: On the possible causes of recent increases in northern hemispheric total ozone from a statistical analysis of satellite data from 1979 to 2003, Atmos. Chem. Phys., 6, 1165–1180, doi:10.5194/acp-6-1165-2006, 2006. 30410, 30413, 30416, 30425
Dobson, G. M.: Origin and distribution of the polyatomic molecules in the atmosphere, Proc. Roy. Soc. Lond. A, 236, 187–193, 1956. 30412
Dunkerton, T. J. and Baldwin, M. P.: Quasi-biennial modulation of planetary-wave fluxes in the Northern Hemisphere winter, J. Atmos. Sci., 48, 1043–1061, 1991. 30414
Fioletov, V.: Estimating the 27-day and 11-year solar cycle variations in tropical upper stratospheric ozone, J. Geophys. Res., 114, D02302, doi:10.1029/2008JD010499, 2009. 30410, 30416
Fioletov, V. E. and Shepherd, T. G.: Seasonal persistence of midlatitude total ozone anomalies, Geophys. Res. Lett., 20, 1417, doi:10.1029/2002GL016739, 2003. 30412
Fioletov, V. E. and Shepherd, T. G.: Summertime total ozone variations over middle and polar latitudes, Geophys. Res. Lett., 32, L04807, doi:10.1029/2004GL022080, 2005. 30416, 30423
Fioletov, V. E., Bodeker, G. E., Miller, A. J., McPeters, R. D., and Stolarski, R.: Global and zonal total ozone variations estimated from ground-based and satellite measurements: 1964–2000, J. Geophys. Res.-Atmos., 107, 4647, doi:10.1029/2001jd001350, 2002. 30417, 30424, 30443
Fioletov, V. E., Labow, G., Evans, R. G., Hare, E. W., Köhler, U., McElroy, C. T., Miyagawa, K., Redondas, A., Savastiouk, V., Shalamyansky, A. M., Staehelin, J., Vanicek, K., and Weber, M.: The performance of the ground-based total ozone network assessed using satellite data, J. Geophys. Res., 113, D14313, doi:10.1029/2008JD009809, 2008. 30443
Frossard, L., Rieder, H. E., Ribatet, M., Staehelin, J., Maeder, J. A., Di Rocco, S., Davison, A. C., and Peter, T.: On the relationship between total ozone and atmospheric dynamics and chem-

ACPD
13, 30407–30452, 2013

istry at mid-latitudes – Part 1: Statistical models and spatial fingerprints of atmospheric dynamics and chemistry, Atmos. Chem. Phys., 13, 147–164, doi:10.5194/acp-13-147-2013, 2013. 30424
Fujiwara, M., Kita, K., Kawakami, S., Ogawa, T., Komala, N., Saraspriya, S., and Suripto, A.: Tropospheric ozone enhancements during the Indonesian forest fire events in 1994 and in 1997 as revealed by ground-based observations, Geophys. Res. Lett., 26, 2417–2420, doi:10.1029/1999GL900117, 1999. 30414
Fusco, A. C. and Salby, M. L.: Interannual variations of total ozone and their relationship to variations of planetary wave activity, J. Climate, 12, 1619–1629, 1999. 30412, 30413
Haigh, J. D.: The effects of solar variability on the Earth's climate, Philos. T. Roy. Soc. A, 361, 95–111, 2003. 30416
Harris, N. R. P., Kyrö, E., Staehelin, J., Brunner, D., Andersen, S.-B., Godin-Beekmann, S., Dhomse, S., Hadjinicolaou, P., Hansen, G., Isaksen, I., Jrrar, A., Karpetchko, A., Kivi, R., Knudsen, B., Krizan, P., Lastovicka, J., Maeder, J., Orsolini, Y., Pyle, J. A., Rex, M., Vanicek, K., Weber, M., Wohltmann, I., Zanis, P., and Zerefos, C.: Ozone trends at northern mid- and high latitudes – a European perspective, Ann. Geophys., 26, 1207–1220, doi:10.5194/angeo-26-1207-2008, 2008. 30410, 30416, 30424, 30425
Hartmann, D. L., Wallace, J. M., Limpasuvan, V., Thompson, D., and Holton, J. R.: Can ozone depletion and global warming interact to produce rapid climate change?, P. Natl. Acad. Sci. USA, 97, 1412–1417, 2000. 30413
Haynes, P. H., Marks, C. J., McIntyre, M. E., Shepherd, T. G., and Shine, K. P.: On the "downward control" of extratropical diabatic circulations by eddy-induced mean zonal forces, J. Atmos. Sci., 48, 651–678, 1991. 30412
Hofmann, D. J. and Solomon, S.: Ozone destruction through heterogeneous chemistry following the eruption of El Chichón, J. Geophys. Res., 94, 5029–5041, 1989. 30410, 30417
Holton, J. R. and Tan, H.-C.: The influence of the equatorial quasi-biennial oscillation on the global circulation at 50 mb, J. Atmos. Sci., 37, 2200–2208, 1980. 30414
Hood, L. L.: The solar cycle variation of total ozone: dynamical forcing in the lower stratosphere, J. Geophys. Res., 102, 1355–1370, 1997. 30410, 30416
Hood, L. L. and Soukharev, B. E.: Quasi-decadal variability of the tropical lower stratosphere: the role of extratropical wave forcing, J. Atmos. Sci., 60, 2389–2403, 2003. 30416
Hood, L. L. and Soukharev, B. E.: Interannual variations of total ozone at northern midlatitudes correlated with EP flux and potential vorticity, J. Atmos. Sci., 62, 3724–3740, 2005. 30410

ACPD
13, 30407–30452, 2013

Kiesewetter, G., Sinnhuber, B.-M., Weber, M., and Burrows, J. P.: Attribution of stratospheric ozone trends to chemistry and transport: a modelling study, Atmos. Chem. Phys., 10, 12073–12089, doi:10.5194/acp-10-12073-2010, 2010. 30413, 30416, 30418, 30423, 30426, 30429, 30443

Kodera, K. and Kuroda, Y.: Dynamical response to the solar cycle: winter stratopause and lower stratosphere, J. Geophys. Res., 1007, 4749, doi:10.1029/2002JD002224, 2002. 30416

Labitzke, K. and van Loon, H.: Some recent studies of probable connections between solar and atmospheric variability, Ann. Geophys., 11, 1084–1094, 1993, http://www.ann-geophys.net/11/1084/1993/. 30416

Labitzke, K. and van Loon, H.: The Stratosphere, Springer-Verlag, New York, 179 pp., 1999. 30415

Lait, L. R., Schoeberl, M. R., and Newman, P. A.: Quasibiennial modulation of the Antarctic ozone depletion, J. Geophys. Res., 94, 1559–11571, 1989. 30414

Lean, J. and Rind, D.: Sun-climate connections: earth's response to a variable sun, Science, 292, 234–236, 2001. 30416

Lee, H. and Smith, A. K.: Simulation of the combined effects of solar cycle, quasi-biennial oscillation, and volcanic forcing on stratospheric ozone changes in recent decades, J. Geophys. Res., 108, 4049, doi:10.1029/2001JD001503, 2003. 30410, 30416

Lindzen, R. S. and Holton, J. R.: A theory of the quasi-biennial oscillation, J. Atmos. Sci., 25, 1095–1107, 1968. 30413

Mäder, J. A., Staehelin, J., Brunner, D., Stahel, W. A., Wohltmann, I., and Peter, T.: Statistical modeling of total ozone: selection of appropriate explanatory variables, J. Geophys. Res.-Atmos., 112, D11108, doi:10.1029/2006jd007694, 2007. 30410, 30424

Mäder, J. A., Staehelin, J., Peter, T., Brunner, D., Rieder, H. E., and Stahel, W. A.: Evidence for the effectiveness of the Montreal Protocol to protect the ozone layer, Atmos. Chem. Phys., 10, 12161–12171, doi:10.5194/acp-10-12161-2010, 2010. 30430

Manzini, E., Giorgetta, M. A., Esch, M., Kornblueh, L., and Roeckner, E.: The influence of sea surface temperatures on the northern winter stratosphere: ensemble simulations with the MAECHAM5 model, J. Climate, 19, 3863–3881, doi:10.1175/JCLI3826.1, 2006. 30415

McCormack, J. P., Hood, L. L., Nagatani, R., Miller, A. J., Planet, W. G., and McPeters, R. D.: Approximate separation of volcanic and 11-year signals in the SBUV-SBUV/2 total ozone record over the 1979–1995 period, Geophys. Res. Lett., 24, 2729–2732, 1997. 30410, 30416

ACPD
13, 30407–30452, 2013

McPeters, R. D., Bhartia, P. K., Haffner, D., Labow, G. J., and Flynn, L.: The version 8.6 SBUV ozone data record: an overviewl, J. Geophys. Res.-Atmos., 118, 8032–8039, doi:10.1002/jgrd.50597, 2013. 30417, 30426, 30429, 30443

Miller, A., Cai, A., Taio, G., Wuebbles, D., Flynn, L., Yang, S.-K., Weatherhead, E., Fioletov, V., Petropavlovskikh, I., Meng, X.-L., Guillas, S., Nagatani, R., and Reinsel, G.: Examination of ozonesonde data for trends and trend changes incorporating solar and Arctic oscillation signals, J. Geophys. Res., 111, D13305, doi:10.1029/2005JD006684, 2006. 30425

Miller, A. J., Hollandsworth, S. M., Flynn, L. E., Tiao, G. C., Reinsel, G. C., Bishop, L., McPeters, R. D., Planet, W. G., DeLuisi, J. J., Mateer, C. L., Wuebbles, D., Kerr, J., and Nagatani, R. M.: Comparisons of observed ozone trends and solar effects in the stratosphere through examination of ground-based Umkehr and combined solar backscattered ultraviolet (SBUV) and SBUV 2 satellite data, J. Geophys. Res., 101, 9017–9021, 1996. 30410, 30416

Molina, M. J. and Rowland, F. S.: Stratospheric sink for chloro-fluoromethanes: chlorine atom catalyzed destruction of ozone, Nature, 249, 820–812, 1974. 30415

Newchurch, M. J., Yang, E.-S., Cunnold, D. M., Reinsel, G. C., Zawodny, J. M., and Russell, J. M.: Evidence for slowdown in stratospheric ozone loss: first stage of ozone recovery, J. Geophys. Res., 108, 4507, doi:10.1029/2003JD003471, 2003. 30425

Newman, P. A., Nash, E. R., and Rosenfield, J.: What controls the temperature of the arctic stratosphere during the spring?, J. Geophys. Res., 106, 19999–20010, 2001. 30412, 30413, 30415

Newman, P. A., Kawa, S. R., and Nash, E. R.: On the size of the Antarctic ozone hole, Geophys. Res. Lett., 31, L21104, doi:10.1029/2004GL020596, 2004. 30416

Newman, P. A., Nash, E. R., Kawa, S. R., Montzka, S. A., and Schauffler, S. M.: When will the Antarctic ozone hole recover?, Geophys. Res. Lett., 33, L12814, doi:10.1029/2005GL025232, 2006. 30419

Newman, P. A., Daniel, J. S., Waugh, D. W., and Nash, E. R.: A new formulation of equivalent effective stratospheric chlorine (EESC), Atmos. Chem. Phys., 7, 4537–4552, doi:10.5194/acp-7-4537-2007, 2007. 30419

Peter, T.: Microphysics and heterogeneous chemistry of polar stratospheric clouds, Annu. Rev. Phys. Chem., 48, 785–822, 1997. 30410, 30417

Plumb, R. A.: The interaction of two internal waves with the mean flow: implications for the theory of the quasi-biennial oscillation, J. Atmos. Sci., 34, 1847–1858, 1977. 30413

Plumb, R. A.: Stratospheric transport, J. Meteor. Soc. Jpn., 80, 793–809, 2002. 30412

ACPD
13, 30407–30452, 2013

Randel, W. J. and Wu, F.: A stratospheric ozone profile data set for 1979–2005: variability, trends, and comparisons with column ozone data, J. Geophys. Res., 112, D06313, doi:10.1029/2006JD007339, 2007. 30416

Randel, W. J. and Cobb, J. B.: Coherent variations of monthly mean column ozone and lower stratospheric temperature, J. Geophys. Res., 99, 5433–5447, 1994. 30414

Randel, W. J., Wu, F., Russell III, J. M., Waters, J. W., and Froidevaux, L.: Ozone and temperature changes in the stratosphere following the eruption of Mt. Pinatubo, J. Geophys. Res., 100, 16753–16764, 1995. 30417

Randel, W. J., Wu, F., and Stolarski, R.: Changes in column ozone correlated with the stratospheric EP flux, J. Meteorol. Soc. Jpn., 80, 849–862, 2002. 30412, 30413, 30415

Reed, R., Campbell, W., Rasmussen, L., and Rogers, D.: Evidence of downward-propagating annual wind reversal in the equatorial stratosphere, J. Geophys. Res., 66, 813–818, 1961. 30413

Reinsel, G. C., Weatherhead, E. C., Tiao, G. C., Miller, A. J., Nagatani, R. M., Wuebbles, D. J., and Flynn, L. E.: On detection of turnaround and recovery in trend for ozone, J. Geophys. Res., 107, 4078, doi:10.1029/2001JD000500, 2002. 30425

Reinsel, G. C., Miller, A. J., Weatherhead, E. C., Flynn, L. E., Nagatani, R. M., Tiao, G. C., and Wuebbles, D. J.: Trend analysis of total ozone data for turnaround and dynamical contributions, J. Geophys. Res., 110, D16306, doi:10.1029/2004JD004662, 2005. 30410, 30425

Rieder, H. E., Staehelin, J., Maeder, J. A., Peter, T., Ribatet, M., Davison, A. C., Stübi, R., Weihs, P., and Holawe, F.: Extreme events in total ozone over Arosa – Part 1: Application of extreme value theory, Atmos. Chem. Phys., 10, 10021–10031, doi:10.5194/acp-10-10021-2010, 2010a. 30424

Rieder, H. E., Staehelin, J., Maeder, J. A., Peter, T., Ribatet, M., Davison, A. C., Stübi, R., Weihs, P., and Holawe, F.: Extreme events in total ozone over Arosa – Part 2: Fingerprints of atmospheric dynamics and chemistry and effects on mean values and long-term changes, Atmos. Chem. Phys., 10, 10033–10045, doi:10.5194/acp-10-10033-2010, 2010b. 30424

Rieder, H. E., Jancso, L. M., Di Rocco, S., Staehelin, J., Mäder, J. A., Peter, T., Ribatet, M., Davison, A. C., De Backer, H., Koehler, U., Krzyścin, J., and Vaníček, K.: Extreme events in total ozone over the northern mid-latitudes: an analysis based on long-term data sets from five European ground-based stations, Tellus B, 63, 860–874, doi:10.1111/j.1600-0889.2011.00575.x, 2011. 30424

ACPD
13, 30407–30452, 2013

Rieder, H. E., Frossard, L., Ribatet, M., Staehelin, J., Maeder, J. A., Di Rocco, S., Davison, A. C., Peter, T., Weihs, P., and Holawe, F.: On the relationship between total ozone and atmospheric dynamics and chemistry at mid-latitudes – Part 2: The effects of the El Niño/Southern Oscillation, volcanic eruptions and contributions of atmospheric dynamics and chemistry to long-term total ozone changes, Atmos. Chem. Phys., 13, 165–179, doi:10.5194/acp-13-165-2013, 2013. 30424

Rind, D.: The sun's role in climate variations, Science, 296, 673–677, 2002. 30416

Rosenlof, K. and Holton, J. R.: Estimates of the stratospheric residual circulation using the downward control principle, J. Geophys. Res., 98, 10465–10479, 1993. 30412

Sato, M., Hansen, J. E., McCormack, M. P., and Pollack, J. B.: Stratospheric aerosol optical depth, J. Geophys. Res., 98, 1850–1990, 1993. 30419

Schnadt Poberaj, C., Staehelin, J., and Brunner, D.: Missing stratospheric ozone decrease at Southern Hemisphere middle latitudes after Mt. Pinatubo: a dynamical perspective, J. Atmos. Sci., 68, 1922–1945, 2011. 30417, 30424

Sinnhuber, B.-M., Sheode, N., Sinnhuber, M., Chipperfield, M. P., and Feng, W.: The contribution of anthropogenic bromine emissions to past stratospheric ozone trends: a modelling study, Atmos. Chem. Phys., 9, 2863–2871, doi:10.5194/acp-9-2863-2009, 2009. 30419

Solomon, S.: Stratospheric ozone depletion: a review of concepts and history, Rev. Geophys., 37, 275–316, 1999. 30409, 30410, 30415, 30417

Solomon, S., Portman, R. W., Garcia, R. R., Thomason, L. W., Poole, L. R., and McCormack, M. P.: The role of aerosol variations in anthropogenic ozone depletion at northern midlatitudes, J. Geophys. Res., 101, 6713–6727, 1996. 30417

Soukharev, B. and Hood, L.: Solar cycle variation of stratospheric ozone: multiple regression analysis of long-term satellite data sets and comparisons with models, J. Geophys. Res., 111, D20314, doi:10.1029/2006JD007107, 2006. 30410, 30416

SPARC: Stratospheric Processes and Their Role in Climate: Assessment of Trends in the Vertical Distribution of Ozone, SPARC Report 1, edited by: Harris, N., Hudson, R., and Phillips, C., SPARC Report no. 1, 1998. 30410, 30417, 30418

SPARC: SPARC CCMVal (Stratospheric Processes and Their Role in Climate), SPARC Report on the Evaluation of Chemistry-Climate Models, edited by: Eyring, V., Shepherd, T. G., and Waugh, D. W., SPARC Report No. 5, WCRP-132, WMO/TD-No. 1526, 478 pp., available at: http://www.atmosp.physics.utoronto.ca/SPARC/ccmval_final/index.php (last access: Nov. 2013), Geneva, 2010. 30418

ACPD
13, 30407–30452, 2013

Staehelin, J., Kegel, R., and Harris, N. R. P.: rend analysis of the homogenized total ozone series of Arosa (Switzerland), 1926–1996, J. Geophys. Res.-Atmos., 103, 8389–8399, 1998. 30424
Staehelin, J., Harris, N. R. P., Appenzeller, C., and Eberhard, J.: Ozone trends: a review, Rev. Geophys., 39, 231–290, 2001. 30409
Steinbrecht, W., Köhler, U., Claude, H., Weber, M., Burrows, J. P., and van der A, R. J.: Very high ozone columns at northern mid-latitudes in 2010, Geophys. Res. Lett., 38, L06803, doi:10.1029/2010GL046634, 2001. 30413, 30424
Steinbrecht, W., Hassler, B., Claude, H., Winkler, P., and Stolarski, R. S.: Global distribution of total ozone and lower stratospheric temperature variations, Atmos. Chem. Phys., 3, 1421–1438, doi:10.5194/acp-3-1421-2003, 2003. 30419
Stolarski, R. S. and Cicerone, R. J.: Stratospheric chlorine: a possible sink for ozone, Can. J. Chem., 52, 1610–1615, 1974. 30415
Stolarski, R. S. and Frith, S. M.: Search for evidence of trend slow-down in the long-term TOMS/SBUV total ozone data record: the importance of instrument drift uncertainty, Atmos. Chem. Phys., 6, 4057–4065, doi:10.5194/acp-6-4057-2006, 2006. 30416, 30417, 30443
Sudo, K. and Takahashi, M.: Simulation of tropospheric ozone changes during 1997–1998 El Niño: meteorological impact on tropospheric photochemistry, Geophys. Res. Lett., 23, 4091–4094, 2001. 30415
Taguchi, M. and Hartmann, D. L.: Increased occurrence of stratospheric sudden warming during El Niño as simulated by WACCM, J. Climate, 19, 324–332, 2006. 30415
Thompson, A. M., Witte, J. C., Hudson, R. D., Guo, H., Herman, J. R., and Fujiwara, M.: Tropical tropospheric ozone and biomass burning, Science, 291, 2128–2132, 2001. 30414
Trenberth, K. E., Caron, J. M., Stepaniak, D. P., and Worley, S.: Evolution of El Niño-Southern Oscillation and global atmospheric surface temperatures, J. Geophys. Res., 107, 4065, doi:10.1029/2000JD000298, 2002. 30415
Tung, K. and Yang, H.: Global QBO in circulation and ozone, Part I: Reexamination of observational evidence, J. Atmos. Sci., 51, 2699–2707, 1994. 30414
van Loon, H. and Labitzke, K.: The Southern Oscillation, Part V: The anomalies in the lower stratosphere of the Northern Hemisphere in winter and a comparison with the quasi-biennial oscillation, Mon. Weather Rev., 115, 357–369, 1987. 30415
Viereck, R. A., Puga, L., McMullin, D., Judge, D., Weber, M., and Tobiska, W. K.: The Mg II index: a proxy for solar EUV, Geophys. Res. Lett., 28, 1343–1346, 2001. 30429

ACPD
13, 30407–30452, 2013

Viereck, R. A., Floyd, L. E., Crane, P. C., Woods, T. N., Knapp, B. G., Rottman, G., Weber, M., Puga, L. C., and DeLand, M. T.: A composite MgII index spanning from 1978 to 2003, Adv. Space Res., 2, S10005, doi:10.1029/2004SW000084, 2004. 30429

Vyushin, D., Fioletov, V., and Shepherd, T.: Impact of long-range correlations on trend detection in total ozone, J. Geophys. Res., 112, D14307, doi:10.1029/2006JD008168, 2007. 30425

Vyushin, D., Shepherd, T., and Fioletov, V.: On the statistical modeling of persistence in total ozone anomalies, J. Geophys. Res., 115, D16306, doi:10.1029/2009JD013105, 2010. 30425, 30426

Weber, M., Lamsal, L. N., Coldewey-Egbers, M., Bramstedt, K., and Burrows, J. P.: Pole-to-pole validation of GOME WFDOAS total ozone with groundbased data, Atmos. Chem. Phys., 5, 1341–1355, doi:10.5194/acp-5-1341-2005, 2005. 30418

Weber, M., Lamsal, L. N., and Burrows, J. P.: Improved SCIAMACHY WFDOAS total ozone retrieval: steps towards homogenising long-term total ozone datasets from GOME, SCIAMACHY, and GOME2, Proc. "Envisat Symposium 2007", Montreux, Switzerland, 23–27 April 2007, ESA SP-636, July 2007, available at: http://envisat.esa.int/envisatsymposium/proceedings/posters/3P4/463281we.pdf (last accessed: November 2013), 2007. 30418

Weber, M., Dikty, S., Burrows, J. P., Garny, H., Dameris, M., Kubin, A., Abalichin, J., and Langematz, U.: The Brewer-Dobson circulation and total ozone from seasonal to decadal time scales, Atmos. Chem. Phys., 11, 11221–11235, doi:10.5194/acp-11-11221-2011, 2011. 30412, 30413, 30418, 30420, 30421, 30426, 30429, 30443

Weber, M., Steinbrecht, W., Long, C. S., Fioletov, V. E., Frith, S. H., Stolarski, R. S., and Newman, P. A.: [Global climate] stratospheric ozone [in state of the climate in 2011], B. Am. Meteorol. Soc., 93, S46–S48, 2012. 30418, 30426, 30429, 30443

WMO: World Meteorological Organization: Global Ozone Research and Monitoring Project, Scientific Assessment of Ozone Depletion: 1998, Report No. 44, World Meteorological Organization, Geneva, 1999. 30410, 30415, 30416, 30417, 30418

WMO: World Meteorological Organization: Global Ozone Research and Monitoring Project, Scientific Assessment of Ozone Depletion: 2002, Report No. 47, World Meteorological Organization, Geneva, 2003. 30410, 30415, 30416, 30417, 30418, 30424

WMO: World Meteorological Organization: Global Ozone Research and Monitoring Project, Scientific Assessment of Ozone Depletion: 2006, Report No. 50, World Meteorological Organization, Geneva, 2007. 30410, 30415, 30416, 30417, 30418, 30424

ACPD
13, 30407–30452, 2013

WMO: World Meteorological Organization: Global Ozone Research and Monitoring Project, Scientific Assessment of Ozone Depletion: 2010, Report No. 52, World Meteorological Organization, Geneva, 2011. 30410, 30415, 30416, 30417, 30418, 30424

Wohltmann, I., Lehmann, R., Rex, M., Brunner, D., and Mäder, J. A.: A process-oriented regression model for column ozone, J. Geophys. Res.-Atmos., 112, D12304, doi:10.1029/2006jd007573, 2007. 30410, 30420, 30424, 30425

Yang, S.-K., Long, C., Miller, A., He, X., Yang, Y., Wuebbles, D., and Tiao, G.: Modulation of natural variability on a trend analysis of updated cohesive SBUV(/2) total ozone, Int. J. Remote Sens., 30, 3975–3986, doi:10.1080/01431160902821924, 2009. 30425

Zeng, G. and Pyle, J. A.: Influence of El Niño Southern Oscillation on stratosphere/troposphere exchange and the global tropospheric ozone budget, Geophys. Res. Lett., 32, L0814, doi:10.1020/2004GL021353, 2005. 30415

Zerefos, C. S., Tourpali, K., Bojkov, R., Balis, D., Rognerund, B., and Isaksen, I.: Solar acticity – total ozone relationships: observations and model studies with heterogeneous chemistry, J. Geophys. Res., 102, 1561–1569, 1997. 30410, 30416

Ziemke, J. R., Chandra, S., McPeters, R. D., and Newman, P. A.: Dynamical proxies of column ozone with applications to global trend models, J. Geophys. Res., 102, 6117–6129, 1997. 30410, 30416

Ziemke, J. R., Chandra, S., Oman, L. D., and Bhartia, P. K.: A new ENSO index derived from satellite measurements of column ozone, Atmos. Chem. Phys., 10, 3711–3721, doi:10.5194/acp-10-3711-2010, 2010. 30415

ACPD
13, 30407–30452, 2013

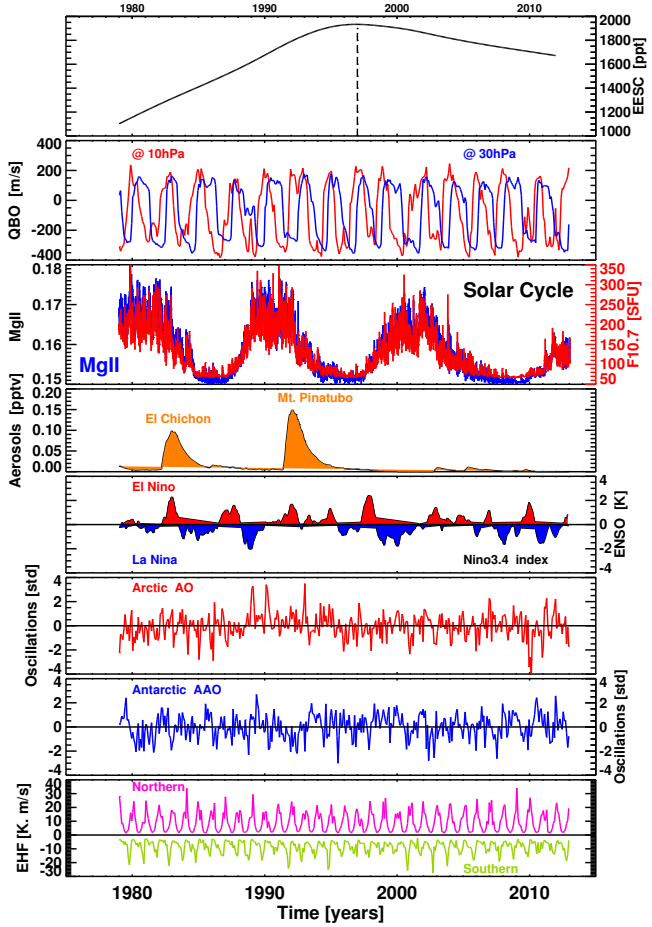

Fig. 1. Please see caption on next page.

ACPD
13, 30407–30452, 2013

Total ozone trends and variability from merged datasets of satellites

W. Chehade et al.

Fig. 1. Time series of the different explanatory variables used in this study are displayed in the panels: stratospheric loading of ODS (first panel) in terms of Equivalent Effective Stratospheric Chlorine (EESC) in pptv. The EESC concentration (black curve) peaked in 1997 and started a slow decline afterwards. Quasi-Biennial Oscillation (QBO) index at 10 hPa (red) and at 30 hPa (blue) are shown in the second panel. The equatorial zonal winds at both levels are out of phase by about $\pi/2$. The third panel displays the 11 yr solar cycle as expressed by the solar flux at 10.7 cm (red) and core-to-wing ratio of the MgII line at 280 nm (blue). Time series of mean optical thickness at 550 nm (orange) to account for volcanic aerosol enhancements are presented in the fourth panel; the dominant features are the 1982 eruption of EL Chicohón and the 1991 eruption of Mt. Pinatubo. Nino 3.4 Index describing the state of the El Niño/Southern Oscillation (ENSO) is shown in panel five: El Niño (red) and La Niña (blue). The next two panels show the teleconnection patterns: Arctic Oscillation (AO) index in red and Antarctic Oscillation (AAO) index in blue.In the last panel, extra-tropical eddy heat flux at 100 hPa averaged over midlatitudes (area weight averaged between 45° N and 75° N) and averaged from October to March in the NH (magenta) and from March to September in the SH (green).

ACPD
13, 30407–30452, 2013

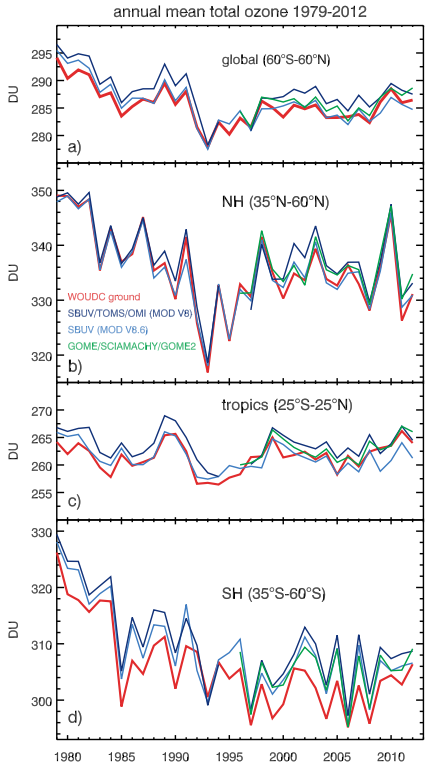

Fig. 2. Annual mean area-weighted total ozone time series of ground-based measurements combining Brewer, Dobson, and filter spectrometer data (red, Fioletov et al., 2002, 2008), the merged SBUV/TOMS/OMI MOD V8.0 (dark blue: Stolarski and Frith, 2006), the merged SBUV/SBUV-2 MOD V8.6 (blue: DeLand et al., 2012; McPeters et al., 2013), and GOME/SCIAMACHY/GOME-2 "GSG" (green, Kiesewetter et al., 2010; Weber et al., 2011, 2012), in the zonal bands: **(a)** 60° N–60° N (global), **(b)** 30° N–60° N (NH), **(c)** 25° S–25° N (tropics), and **(d)** 35° S–60° S (SH) zonal bands.

ACPD
13, 30407–30452, 2013

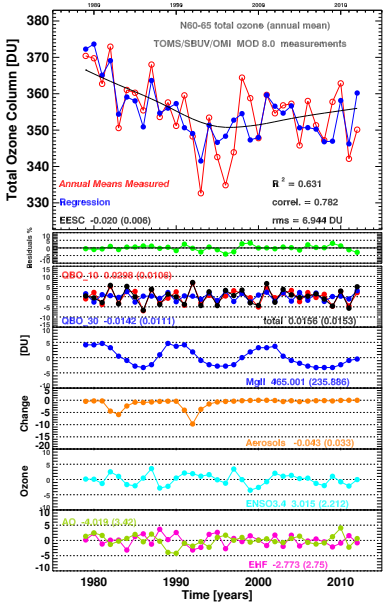

Fig. 3. Annual mean total ozone variations for 60° N–65° N in DU (TOMS/SBUV/OMI V8.0 dataset from 1979–2012) and magnitude of contributing factors obtained by multiple linear regressions. Top panel: observed total annual mean data (red), corresponding fit (blue) and the EESC curve (black). Green line marks the residuals between the observed ozone and regressed time series (second panel). Bottom panels show the contributions from: QBO at 10 hPa (red), at 30 hPa (blue) and total effect (black), blue: 11 yr solar cycle (MgII index); orange: enhanced stratospheric aerosols; turquoise: ENSO (3.4 index), eddy heat flux in magenta and AO/AAO oscillation in lime-green, respectively. The correlation between the observed and regressed ozone (R), coefficient of determination (R^2) and residual mean square (rms) are indicated in the first panel. The regression coefficients of various proxies along with the standard deviation (in brackets) are also indicated in each panel.

ACPD
13, 30407–30452, 2013

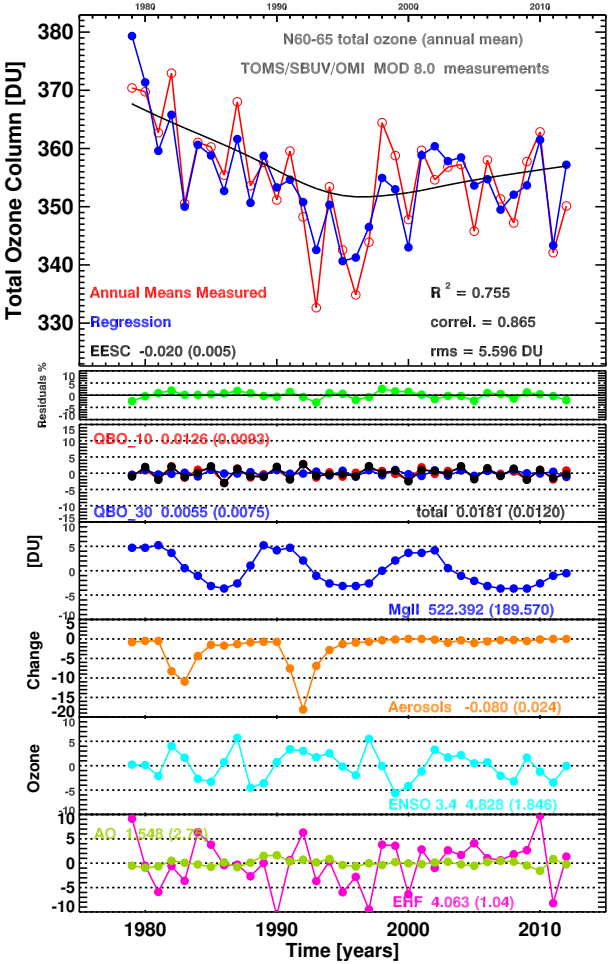

Fig. 4. Same as Fig. 3, except for the wintertime mean eddy heat flux replacing the ozone variability weighted annual mean EHF.

ACPD
13, 30407–30452, 2013

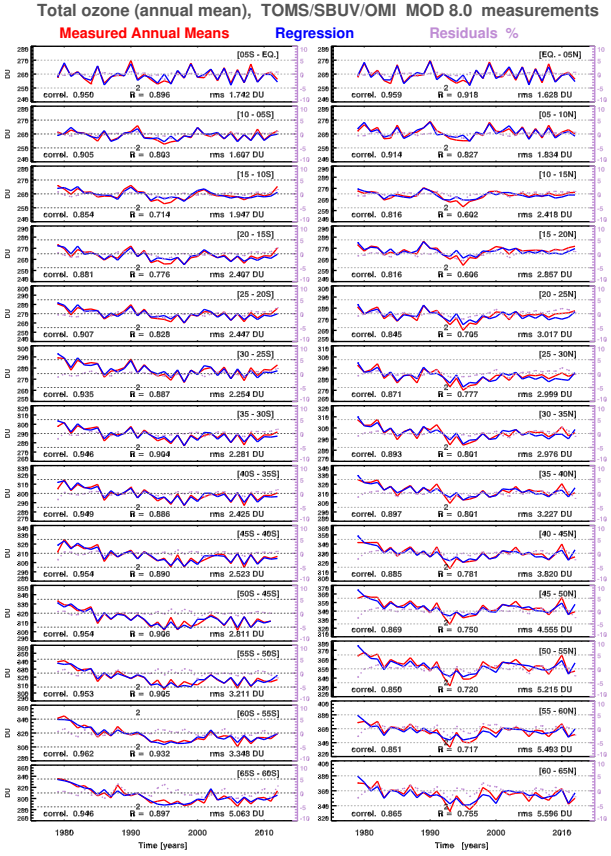

Fig. 5. Observed TOMS/SBUV/OMI V8.0 (red) annual zonal mean total ozone columns for 5° wide latitude bands from 65° S to 65° N and regressed (blue) ozone obtained from regression models (with winter mean EHF dynamical proxy). The right hand scale in each panel gives the residuals in percent (violet). The correlation, R^2 and rms are also noted for each latitude band.

ACPD
13, 30407–30452, 2013

Total ozone trends and variability from merged datasets of satellites

W. Chehade et al.

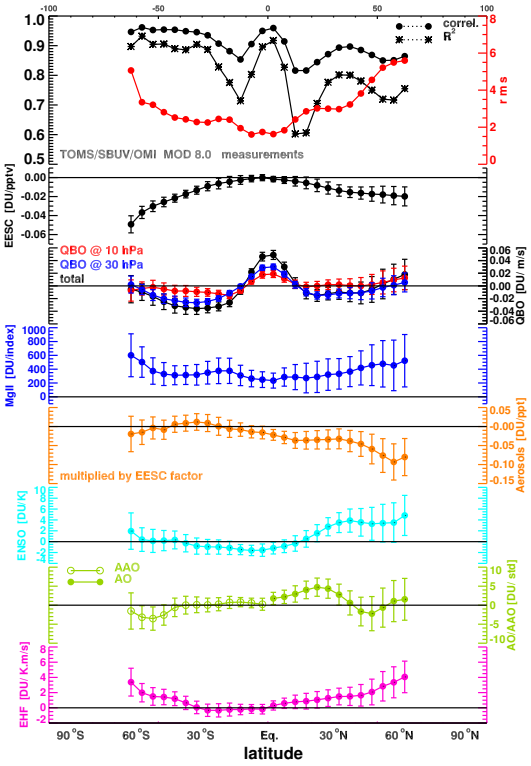

Fig. 6. (Top panel) the correlation, R^2 and rms calculated from multiple linear regression of 1979–2012 merged TOMS/SBUV/OMI 5° latitude zonal annual mean total ozone from 65° S to 65° N (results based on regression Eq. (1) with wintertime EHF dynamical proxy). The fitting coefficients of the different explanatory variables used in this study for each latitude band are displayed in respective colors as in Figs. 3 and 4. Error bars indicate the statistical significance at two sigma level.

ACPD
13, 30407–30452, 2013

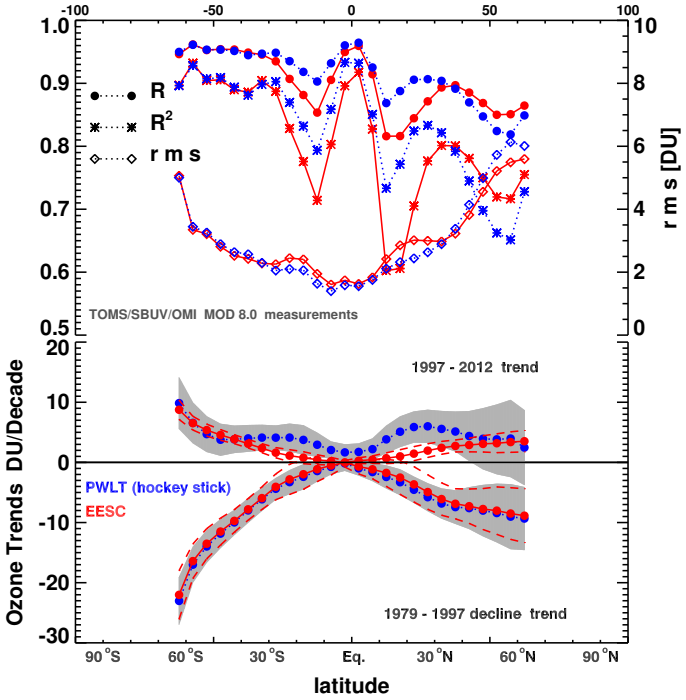

Fig. 7. (Top panel) zonal distribution of the correlation, R^2 and rms estimated for the 1979–2012 TOMS/SBUV/OMI V8.0 merged dataset from regression model based on Eq. (1) in red and the piecewise linear trend (PWLT or hockey stick) model in blue. (bottom panel) Zonal distribution of the linear trend of ozone in DU decade^{-1} units calculated for the EESC-based declining part of EESC during 1979–1997 and for the increasing part of EESC during 1997–2012 (red) as well as the trends before and after the ODS turnaround (1997) calculated by the PWLT model (blue). The statistical significance at two sigma level is indicated as grey shades for PWLT and dashed lines for EESC.

ACPD
13, 30407–30452, 2013

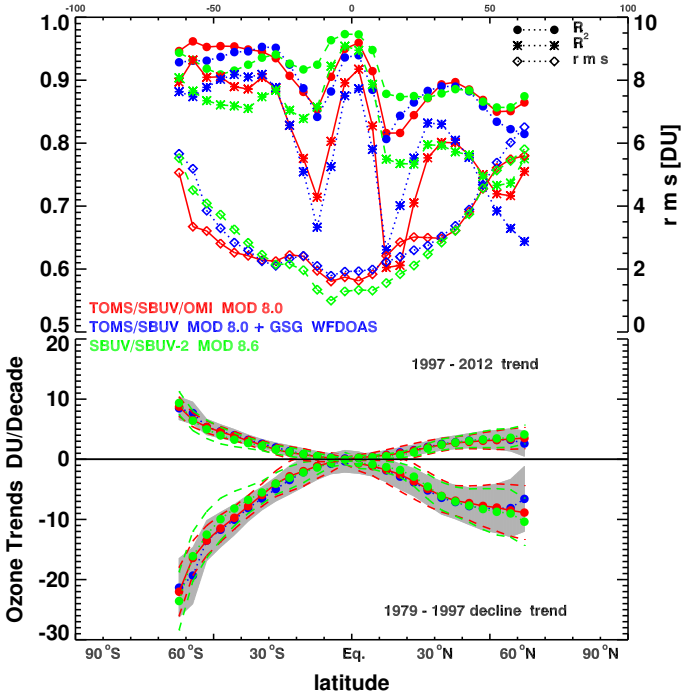

Fig. 8. (Top panel) zonal distribution of the correlation, R^2 and rms estimated for zonal merged GSG data (July 1995–December 2012) combined with TOMS/SBUV Mod V8.0 data (January 1979–June 1995) displayed in blue, SBUV/SBUV-2 MOD 8.6 ozone data (1979–2012) in green and TOMS/SBUV/OMI Mod V8.0 merged data (1979–2012) in red. The results refer to analysis based on regression Eq. (1) using wintertime EHF dynamical proxy. (bottom panel) The EESC-based trends representing the decline from 1979 till 1997 (negative values) and and increase after 1997 (positive values) are displayed for all ozone datasets. Grey shades indicate the statistical significance at two sigma level for TOMS/SBUV/OMI + GSG merged data, red dashed lines for TOMS/SBUV/OMI MOD 8.0 and green dashed lines for the SBUV/SBUV-2 MOD 8.6 dataset.

ACPD
13, 30407–30452, 2013

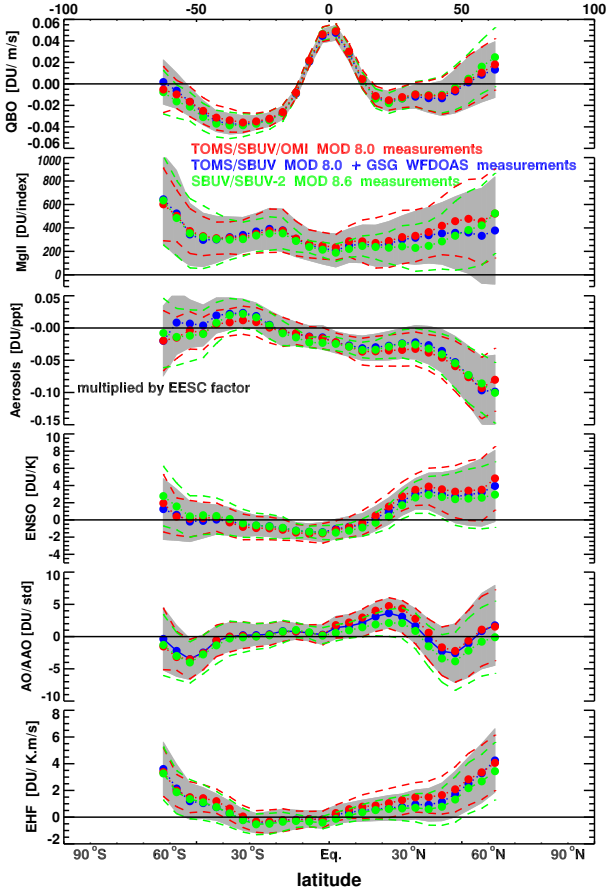

Fig. 9. The fitting coefficients of the different explanatory variables used in the regression analysis of the different merged datasets. The statistical significance at two sigma level is displayed in respective colors as in Fig. 8.

ACPD
13, 30407–30452, 2013

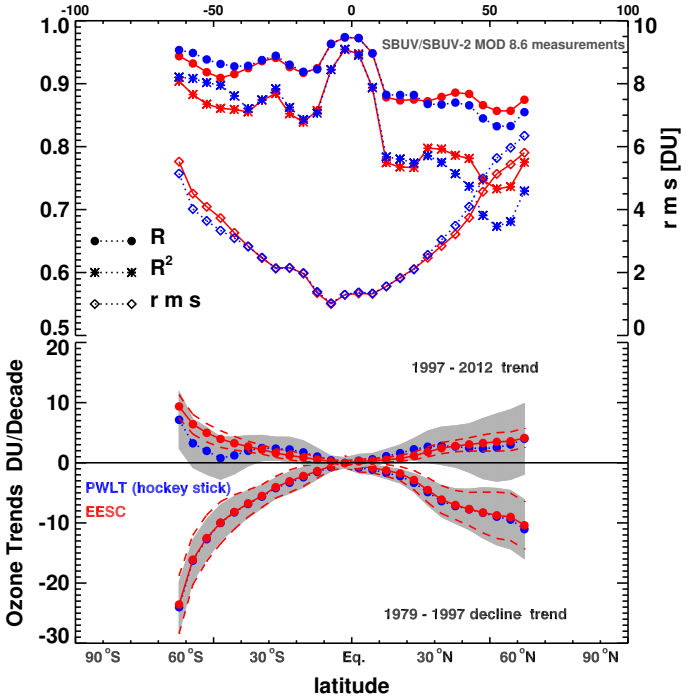

Fig. 10. Same as Fig. 7, but for SBUV/SBUV-2 MOD 8.6 dataset.

ACPD
13, 30407–30452, 2013

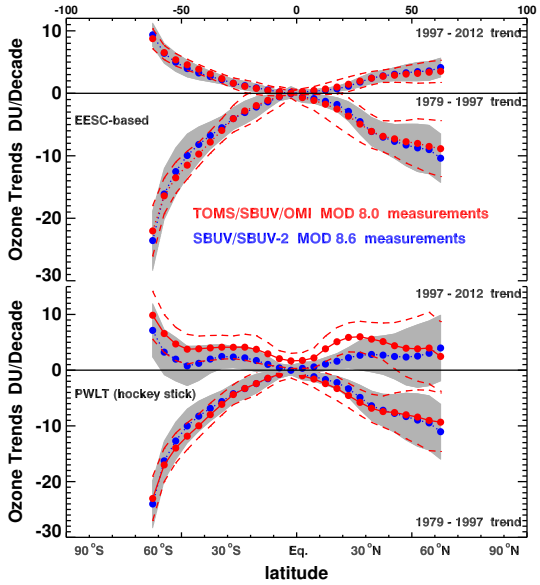

Fig. 11. Comparisons between EESC and PWLT trends before and after 1997 for the MOD V8.0 (red) and MOD V8.6 (blue) total ozone data.

ACPD
13, 30407–30452, 2013